The Journal of Navigation (2026), **79**:1-2 40–55
doi:10.1017/S0373463326101532

CAMBRIDGE UNIVERSITY PRESS

RESEARCH ARTICLE

Line-of-sight based great-circle route track-keeping control

Guoshuai Li[1,2], Guilong Li[1], Xianku Zhang[1,2], Shimiao Wang[1] and Zilong Xie[1]

[1]Navigation College, Dalian Maritime University, China
[2]State Key Laboratory of Maritime Technology and Safety, Dalian Maritime University, China
Corresponding author: Xianku Zhang; Email: zhangxk@dlmu.edu.cn

Received: 23 April 2025; **Revised:** 09 December 2025; **Accepted:** 17 March 2026; **First published online:** 27 April 2026

Keywords: Great circle route; guidance; LOS algorithm; Mercator chart; track keeping control

Abstract

To address the challenges of long voyages and the significant effects of Earth's curvature on ocean navigation, this paper proposes, for the first time, a guidance and control strategy for great-circle routes based on Mercator projection nautical charts. First, a guidance strategy for great-circle routes is designed by combining the traditional line-of-sight (LOS) algorithm with spherical triangles. Tracking control is subsequently achieved through the integration of a closed-loop gain-scheduling algorithm. Next, the vessel's position is transformed from a planar map to a Mercator projection nautical chart to better meet the practical needs of maritime engineering. Finally, the effectiveness of the designed guidance and control algorithm is verified through simulations. The experimental results show that the proposed guidance and control strategy can significantly enhance the stability of the vessel along the great-circle route, reduce navigation time and lower fuel consumption, demonstrating high navigation efficiency and economy.

1. Introduction

As the marine environment becomes more complex and shipping demand keeps rising, ship track-keeping control technology is encountering unparalleled challenges. Traditional path planning methods, although they have met past navigation requirements to some extent, have gradually become a key factor restricting the sustainable development of the shipping industry due to their efficiency bottlenecks in long-distance navigation and insufficient adaptability to complex environments (Hondorp et al., 2017). In the context of the global shipping industry's accelerated transition towards green and low-carbon development, ship track-keeping control technology needs not only to improve navigation efficiency, but also to focus on energy conservation and emission reduction. Therefore, exploring a new type of track-keeping control method is not only an inevitable trend of technological development, but also an urgent need to achieve efficient shipping (Chen et al., 2004). This research, targeting the development of ocean track-keeping control techniques to tackle these challenges, is a vital component of Ocean Engineering and substantially promotes the progress of sustainable maritime technologies.

In this context, numerous researchers have extensively investigated and explored the topic of track-keeping control. A computational fluid dynamics (CFD) model using the unsteady Reynolds-averaged Navier–Stokes (URANS) solver was developed by Kim et al. (2023), combined with a line-of-sight (LOS) guidance algorithm, for track-keeping problems in autonomous marine navigation, especially for performance prediction under wave conditions. Kjerstad and Coates (2024) proposed a novel LOS guidance law for marine surface vessels. This method addresses existing limitations by improving the crab-angle update law, incorporating feedback and optimising its coupling with the heading control system, thereby significantly enhancing track-keeping performance and establishing a new benchmark in this research domain. Furthermore, Dai et al. (2023) presented a three-dimensional track-keeping mechanism for multi-articulated robotic fish, using an adaptive line-of-sight (ALOS) method enhanced

© The Author(s), 2026. Published by Cambridge University Press on behalf of The Royal Institute of Navigation

https://doi.org/10.1017/S0373463326101532 Published online by Cambridge University Press

with a barrier function. The system featured an optimised ALOS guidance approach and incorporated a nonlinear disturbance observer (NDOB) to compensate for the sideslip angle. Additionally, it incorporated three nested-loop controllers for velocity, yaw angle and depth regulation. An enhanced three-dimensional LOS guidance law and a simplified time-delay controller were introduced by Yu et al. (2020) for the three-dimensional integrated route-following control of a six-degree-of-freedom underactuated marine vehicle. Simulation results validated their effectiveness and robustness. In the further exploration of control methods, Meng et al. (2024) created a three-dimensional track-keeping control framework for a six-degree-of-freedom underactuated maritime vehicle, using a LOS guidance scheme combined with a sliding mode controller with fuzzy logic. The track-keeping control scheme was verified by simulations and water tank experiments. An innovative adaptive fast non-singular terminal sliding mode control strategy for track keeping of underpowered unmanned surface vessels (USVs) was introduced by Fan et al. (2021). This approach was built on an enhanced LOS control principle, integrating a diminished-order extended state observer (ESO) to estimate the varying sizable drift bearing. A rapid non-singular terminal sliding mode scheme was developed to boost the system's robustness and precision. Moreover, an supplementary dynamic mechanism was added to tackle the problem of saturation of actuators. Fossen (2022) proposed a ship track-keeping control scheme based on the extended Kalman filter (EKF). This method used the position information from the Global Navigation Satellite System (GNSS) to measure the ship's course over ground (COG) and speed over ground (SOG). It combined the proportional LOS guidance law with a heading autopilot to achieve the following path. In response to the issues of unknown dynamics, unmeasurable velocity and external deviations, Fu and Wang (2023) presented a track-keeping control approach using a finite-time extended state observer (FTESO) to calculate velocity and perturbations. This method combined the LOS guidance law with a safety assurance auxiliary system to ensure that the system converged to zero within a finite time and maintained stability. It was designed for track keeping in complex manoeuvres. Lee et al. (2022) developed an adaptive backstepping-based route-following control method for underactuated catamarans, tackling the track keeping issue in the face of unknown dynamics and time-varying disturbances. A track-keeping control method for USV based on reinforcement learning was introduced by Martinsen et al. (2020). This method integrated model identification and optimised feedback strategies, enabling track keeping under various operating conditions. Furthermore, Mo et al. (2024) proposed an adaptive LOS navigation method based on a finite-limited slip angle observer to earn exacting planar track keeping for biomimetic robotic fish. This method adjusted the LOS guidance in real time based on cross-track error and used a finite-time observer to estimate the slip angle to correct the target yaw angle. The yaw tracking was ultimately achieved through a PID controller. Li et al. (2025) proposed an improved extended-state-observer based line-of-sight (IELOS) guidance law for autonomous underwater helicopter (AUH) track keeping. It incorporates a nonlinear tracking differentiator and an anti-saturation controller to improve tracking accuracy and thrust control. Zhang et al. (2024) introduced a heterogeneous collaborative track-keeping control approach that merges optimised iterative sliding mode control with an extended state observer, enabling high-precision track keeping and robust disturbance rejection for unmanned surface vessels and underwater vehicles. Li et al. (2024) explored the cooperative track-keeping control algorithm between USV and unmanned aerial vehicles (UAVs), thereby further extending the research in the field of track keeping. Liu and Zhang (2024) proposed a new control strategy for USV track keeping in low-speed harbour missions. The strategy improves stability and performance in disturbed environments. Tanakitkorn et al. (2024) introduced the unified line-of-sight (ULOS) guidance algorithm for USV waypoint navigation. It addresses the integral wind-up issue and incorporates sway velocity-based heading compensation to enhance sharp turn performance. These research findings demonstrate that in ship track-keeping control technology, integrating advanced control strategies and algorithms can effectively enhance the accuracy, robustness and adaptability of track keeping. This lays a solid foundation for the green and efficient shipping of intelligent vessels.

However, traditional ship navigation strategies mainly rely on constant course navigation (Stuart, 2017), where ships maintain a fixed heading during the voyage. This method is simple to operate and

https://doi.org/10.1017/S0373463326101532 Published online by Cambridge University Press

convenient to apply. Its drawbacks are increasingly evident in long-distance oceanic voyages (Earle, 2005). Since the constant course line does not fully account for the spherical shape of the Earth, ships often need to take longer routes. This not only increases the distance travelled and extends the voyage time, but also leads to additional fuel consumption and operational costs (Chen et al., 2014). As navigation technology advances swiftly and the demand for navigation efficiency and economic benefits grows, the concept of the great-circle route has come into being (Zheng et al., 2021). The great-circle path represents the minimum distance from one point to another on the globe's surface, leveraging the Earth's spherical shape to offer the most efficient theoretical navigation path (Liu et al., 2023). Compared with constant course navigation, the great-circle route can remarkably reduce distance and shorten voyage time in long-distance navigation, thereby cutting fuel consumption and operational costs while enhancing shipping companies' economic benefits and market competitiveness (Liu et al., 2024a). However, due to the curvature of the Earth's surface and the varying angles of intersection with meridians, it is impractical to strictly follow a great-circle arc in actual navigation. Instead, the great-circle arc is divided into several smaller segments, with each segment approximated by a constant course line (Liu et al., 2024b). To enable ships to navigate precisely along great-circle routes, it is necessary to develop efficient navigational algorithms and control strategies. These advancements will ensure that ships can stably and accurately track great-circle routes in complex marine environments (Do, 2016).

Based on the existing literature, this paper proposes great-circle route control and control strategy based on the Mercator projection nautical chart. The contributions of this paper can be summarised as follows:

(1) A guidance strategy for the great-circle route has been developed through the analysis of spherical triangles. This overcomes the limitation of traditional navigation methods that cannot achieve continuous heading adjustments for ships, ensuring that ships can stably navigate along the arc of the great circle between two points.
(2) The ship's position is transformed from a planar map to a Mercator projection nautical chart, which better meets the practical needs of marine engineering.

The arrangement of the remaining chapters is listed as follows. Section 2, Mathematical Model of Ship Motion, discusses the ship model selected for the experiments in this thesis. Section 3, Guidance and Control, covers the main content of this thesis, including the improvement of the LOS algorithm, controller design, and coordinate transformation. In Section 4, Simulation and Experiment, the improved algorithm is tested with the latitude and longitude coordinates of two points and compared with other methods. Section 5, Conclusion, summarises the advantages and implications of the research presented in this paper.

2. Mathematical model of ship motion

The ship model employed in this paper is the Nomoto model, which is one of the most extensively used linear mathematical models in ship motion control. It can ensure high accuracy in the design of linear controllers and simple system simulations (Zhang et al., 2020). The derivation process is as follows.

When analysing ship manoeuvring motion, if only the sway velocity v and yaw angular velocity r are considered as the two degrees of freedom, the corresponding linear equations are

$$\begin{bmatrix} \dot{v} \\ \dot{r} \end{bmatrix} = \begin{bmatrix} b_{11} & b_{12} \\ b_{21} & b_{22} \end{bmatrix} \begin{bmatrix} v \\ r \end{bmatrix} + \begin{bmatrix} c_{11} \\ c_{21} \end{bmatrix} \delta \tag{1}$$

where δ represents the rudder angle input, $\dot{v}$ represents the first time derivative of the drift velocity and $\dot{r}$ stands for the first time derivative of the yaw rate. The coefficients $b_{11}, b_{12}, b_{21}, b_{22}, c_{11}, c_{21}$ are defined

https://doi.org/10.1017/S0373463326101532 Published online by Cambridge University Press

by the fundamental parameters of the ship. They can be transformed into a straightforward equation that characterises the yaw response to rudder action,

$$T_1T_2\ddot{r} + (T_1 + T_2)\dot{r} + r = K_0\delta + K_0T_3\dot{\delta} \tag{2}$$

where $\dot{\delta}$ indicates the first time derivative of the rudder angle, $\ddot{r}$ denotes the second time derivative of the yaw rate and K_0, T_1, T_2, T_3 are all manoeuvrability indices. Under normal circumstances, T_1 is greater than T_2. However, the value of T_3 is usually comparable to that of T_2.

Applying the Laplace transform of Equation (2) and assuming the initial state $\dot{r}(0) = 0, r(0) = 0, \delta(0) = 0$ holds, we obtain the following transfer function:

$$G_{r\delta}(s) = \frac{r(s)}{\delta(s)} = \frac{K_0(1 + T_3s)}{(1 + T_1s)(1 + T_2s)} \tag{3}$$

In this equation, s is the Laplace operator.

Based on the relationship $\dot{\psi} = r$, we can derive the corresponding equation:

$$G_{\psi\delta}(s) = \frac{\psi(s)}{\delta(s)} = \frac{K_0(1 + T_3s)}{s(1 + T_1s)(1 + T_2s)} \tag{4}$$

A remarkable simplification work has been carried out on Equation (4), reducing the complex second-order transfer function to a first-order one. The starting point of this simplification is based on the understanding that for such transportation vehicles having high inertia characteristics, their dynamic behaviour in the low-range frequency is particularly important (Lan et al., 2023). Therefore, when dealing with the relevant equations, by choosing under low-frequency conditions, s tends to 0 corresponds to the low-frequency range of ship motion, which is precisely the frequency range of primary concern for heading control. For high-inertia ships, low-frequency dynamics dominate and high-frequency dynamics can be reasonably neglected. So, when $s = j\omega$ approaches 0 and using a well-known approximation: when x approaches 0, $(1 - x) \approx 1/(1 + x)$ holds, and ignoring second- and third-order small quantities, we derive the following:

$$G_{\psi\delta}(s) = \frac{K_0}{s(1 + T_0s)} \tag{5}$$

where $T_0 = T_1 + T_2 - T_3$ is present, and Equation (5) can also be written in the following differential equation form:

$$T_0\ddot{\psi} + \dot{\psi} = K_0\delta \tag{6}$$

In this formula, $\dot{\psi}$ represents the first-order derivative of the heading angle ψ with respect to time and $\ddot{\psi}$ denotes the second-order derivative of the heading angle ψ with respect to time.

Dividing both sides of Equation (6) by T_0,

$$\ddot{\psi} + \frac{1}{T_0}\dot{\psi} = \frac{K_0}{T_0}\delta \tag{7}$$

In the case of some statically unstable vessels, the second term on the left-hand side of Equation (7), $\dot{\psi}/T_0$, requires replacement by the nonlinear term $(K/T)H(\dot{\psi})$, and

$$H(\dot{\psi}) = \alpha\dot{\psi} + \beta\dot{\psi}^3 \tag{8}$$

Thus, a nonlinear second-order model for ship manoeuvring response is derived,

$$\ddot{\psi} + \frac{K_0}{T_0}\left(\alpha\dot{\psi} + \beta\dot{\psi}^3\right) = \frac{K_0}{T_0}\delta \tag{9}$$

https://doi.org/10.1017/S0373463326101532 Published online by Cambridge University Press

where ψ is the directional angle, δ represents the rudder deflection angle, K_0, T_0 denotes the ship's agility index and α, β is the nonlinear parameter (Zhu et al., 2025).

This model not only accurately captures the response characteristics of ship motion, but also, compared with the second-order equation, is more concise in form (Yin & Wang, 2021). This model is extensively employed in the development of ship automatic control systems for two key reasons. First, its frequency response in the low-frequency range is almost identical to that of more complex higher-order models. Second, controllers designed based on this model have a simpler structure, reducing the complexity of implementation (Lu et al., 2024).

3. Guidance and control

3.1. LOS guidance principle

The approach adopted in this research is an enhanced LOS guidance technique. It calculates the line-of-sight angle between the target and the vessel, while using sensors to continuously monitor the vessel's real-time position, heading and deviation from the predefined route. Based on this information, it produces control commands to steer the vessel along the intended path. As depicted in Figure 1, consider the current position coordinates of the vessel to be $P(x, y)$, $W_1(x_1, y_1)$, $W_2(x_2, y_2), \ldots,$ $W_i(x_i, y_i)$, which are the predetermined navigation points. Here, $W_1(x_1, y_1)$, $W_2(x_2, y_2)$ represent the present intended trajectory section to be navigated. The implementation of track-keeping control requires two steps. First, it is necessary to determine the tracking error y_e. Then, the location of the tracking target is updated correspondingly. The target is situated at a point Δ ahead of the perpendicular foot. Based on the position of P_{los}, the desired course ψ_d of the ship is updated in real time. The process of searching for a new ψ_d continues until the vessel reaches W_2. The heading angle of the tracked route segment in the geodetic coordinate system can be expressed as

$$\psi_c = \arctan((y_2 - y_1)/(x_2 - x_1)) \tag{10}$$

Here, ψ_c is the direction of the route, which can be described as the direction from the starting point to the destination.

In the track keeping, the longitudinal error and lateral error represent the degree to which the current point deviates from the reference path:

$$\begin{bmatrix} x_e \\ y_e \end{bmatrix} = R^{\mathrm{T}}(\psi_c) \begin{bmatrix} x - x_h \\ y - y_h \end{bmatrix} \tag{11}$$

where $P(x, y)$ is the current position coordinate of the vessel, and $W_h(x_h, y_h)$ is the nearest point on the tracking route segment, x_e denotes the longitudinal error of the ship's current position relative to the planned track and y_e indicates the lateral error of the ship's current position relative to the planned track.

The rotation matrix is used to convert the geodetic coordinate system to the path coordinate system to represent the errors,

$$R^{\mathrm{T}}(\psi_c) = \begin{bmatrix} \cos\psi_c & \sin\psi_c \\ -\sin\psi_c & \cos\psi_c \end{bmatrix} \tag{12}$$

By substituting the rotation matrix into Equation (11),

$$\begin{bmatrix} x_e \\ y_e \end{bmatrix} = \begin{bmatrix} \cos\psi_c & \sin\psi_c \\ -\sin\psi_c & \cos\psi_c \end{bmatrix} \begin{bmatrix} x - x_h \\ y - y_h \end{bmatrix} \tag{13}$$

https://doi.org/10.1017/S0373463326101532 Published online by Cambridge University Press

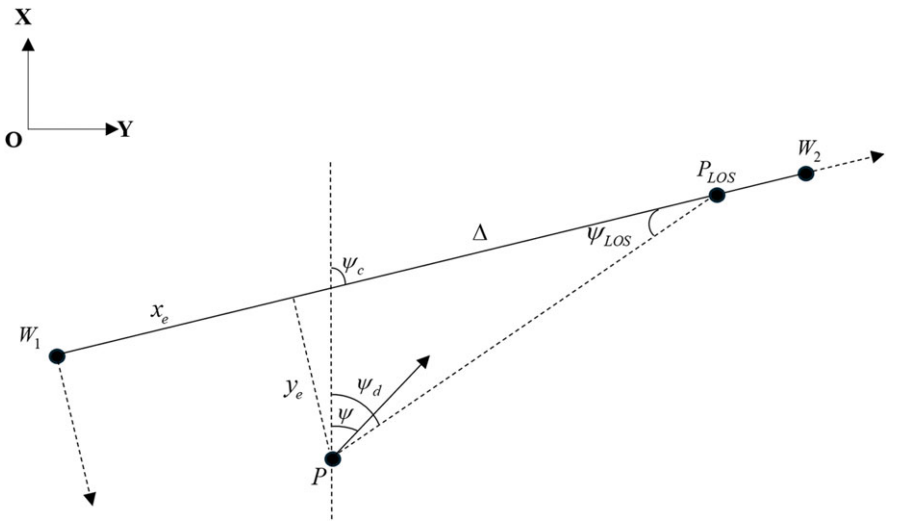


Figure 1. *Schematic diagram of the LOS algorithm principle.*

After expansion, it becomes

$$\begin{aligned} x_e &= (x - x_h)\cos\psi_c + (y - y_h)\sin\psi_c \\ y_e &= -(x - x_h)\sin\psi_c + (y - y_h)\cos\psi_c \end{aligned} \tag{14}$$

The vessel stably converges to the target point P_{los} and continues to track along the path. The desired heading ψ_d is given by

$$\psi_d = \psi_c - \psi_{los} = \psi_c - \arctan\left(y_e/\Delta\right) \tag{15}$$

Here, ψ_d represents the desired heading in the traditional LOS algorithm. However, the desired heading after the algorithm improvement will be denoted by C_T.

3.2. Algorithm improvement

In this part, the original rhumb line course and distance between two waypoints in the LOS algorithm are replaced by the great-circle course and great-circle distance. As a result, the planar triangle used in the conventional LOS computation is transformed into a spherical triangle and all subsequent LOS calculations are carried out on the spherical surface. The specific process is as follows.

(1) Calculate the great-circle course and distance. The LOS guidance algorithm is mostly used for controlling the tracking of a ship sailing along a rhumb line, which means the ship sails along a straight line between two points. In the projection model, the Earth is inherently an ellipsoid; however, to simplify the calculation process and meet the accuracy requirements of common marine engineering applications, this paper assumes the Earth to be a perfect sphere. Based on this spherical model, this study proposes an improved control procedure, enabling the ship to sail along the shortest path between two points on the Earth's surface, namely the great-circle route. Assume the coordinates of the starting point and the destination point are $W_1(\varphi_1, \lambda_1)$ and $W_2(\varphi_2, \lambda_2)$, respectively, as shown in Figure 2.

Using the spherical triangle formula to calculate the initial great-circle course at the point W_1 between the starting and ending points, the formulae for calculating the great-circle distance and course are as follows:

$$\cos S = \sin\varphi_1 \sin\varphi_2 + \cos\varphi_1 \cos\varphi_2 \cos D\lambda \tag{16}$$

https://doi.org/10.1017/S0373463326101532 Published online by Cambridge University Press

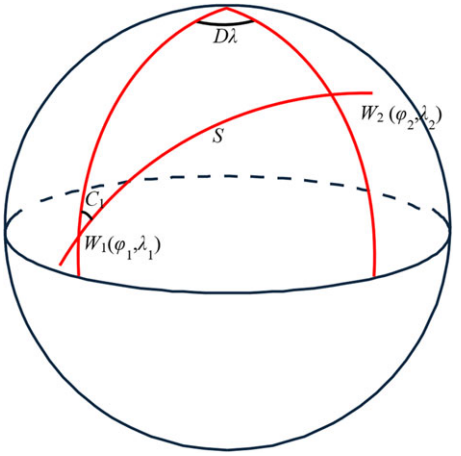


Figure 2. *Schematic diagram of great-circle course and distance calculation.*

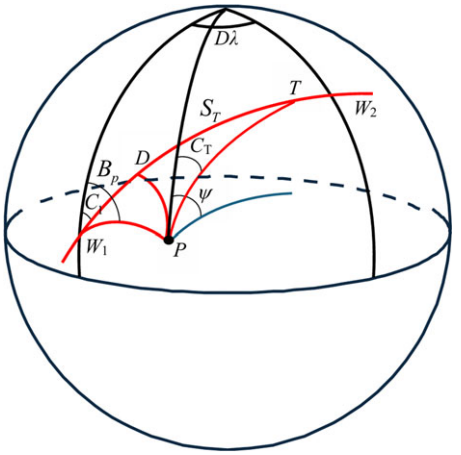


Figure 3. *Schematic diagram of the improved LOS algorithm.*

$$\tan C_1 = \frac{\sin\varphi_2 \cos\varphi_1 - \cos\varphi_2 \sin\varphi_1 \cos D\lambda}{\cos\varphi_2 \sin D\lambda} \tag{17}$$

Here, φ_1 is the latitude of the starting point, the latitude of the destination point is represented by φ_2, $D\lambda$ represents the difference in longitude between the starting and destination points, where C_1 denotes the initial great-circle course.

(2) Calculate the coordinates of the point closest to the present location of the ship. Assuming the ship's current coordinates is $P(\varphi_P, \lambda_P)$, as shown in Figure 3, the great circle interval from the current ship position to W_1 is S_P,

$$\cos S_P = \sin\varphi_1 \sin\varphi_P + \cos\varphi_1 \cos\varphi_P \cos D\lambda_P \tag{18}$$

https://doi.org/10.1017/S0373463326101532 Published online by Cambridge University Press

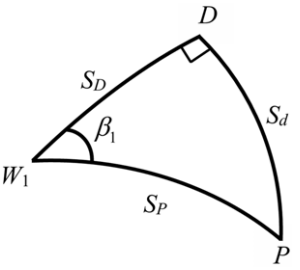


Figure 4. *Schematic diagram of the spherical triangle.*

$$\tan \beta_P = \frac{\sin \varphi_P \cos \varphi_1 - \cos \varphi_P \sin \varphi_1 \cos D\lambda_P}{\cos \varphi_P \sin D\lambda_P} \tag{19}$$

where $D\lambda_P$ is the difference in longitude from the starting point to the present location of the ship; φ_P represents the latitude of the vessel's present coordinates; λ_P represents the longitude of the present location of the ship; S_P indicates the great-circle distance from the starting point to the present location of the ship; and β_P represents the great-circle bearing of point P relative to pointW_1.

At this point, a perpendicular line is extended from the current position, point P, to the great-circle route W_1W_2, with the foot of the perpendicular being point $D(\varphi_D, \lambda_D)$. This forms a spherical right triangle PDW_1, as shown in Figure 4. Therefore,

$$\beta_1 = \beta_P - C_1 \tag{20}$$

$$\sin S_d = \sin \beta_1 \sin S_P \tag{21}$$

$$\sin S_D = \tan S_d \tan(90^\circ - \beta_1) \tag{22}$$

where S_d is the perpendicular distance from P to D; S_D denotes the distance from W_1 to D; β_1 represents the angular separation between the two great-circle arcs W_1W_2 and W_1P.

The coordinates of the point D and the great-circle course can be calculated using the following formulae:

$$\cos \varphi_D = \sin \varphi_1 \sin S_D + \cos \varphi_1 \cos S_D \cos C_1 \tag{23}$$

$$\cos D\lambda_D = \frac{\cos S_D - \sin \varphi_1 \sin \varphi_D}{\cos \varphi_1 \cos \varphi_D} \tag{24}$$

$$\lambda_D = \lambda_1 + D\lambda_D \tag{25}$$

$$\tan C_D = \frac{\sin \varphi_2 \cos \varphi_D - \cos \varphi_2 \sin \varphi_D \cos|\lambda_2 - \lambda_D|}{\cos \varphi_D \sin|\lambda_2 - \lambda_D|} \tag{26}$$

where $D\lambda_D$ is the difference in longitude from the starting point to point D; φ_D denotes the latitude of point D; λ_D represents the longitude of point D; and C_D is the great-circle course at point D.

(3) Calculate the target point coordinates and the desired course. Let the tracking target be located at a point $T(\varphi_T, \lambda_T)$, which is a great-circle distance S_T ahead of the perpendicular foot $D(\varphi_D, \lambda_D)$. The value of S_T is determined through multiple experiments,

$$\cos \varphi_T = \sin \varphi_D \sin S_T + \cos \varphi_D \cos S_T \cos C_D \tag{27}$$

$$\cos D\lambda_T = \frac{\cos S_T - \sin \varphi_D \sin \varphi_T}{\cos \varphi_D \cos \varphi_T} \tag{28}$$

https://doi.org/10.1017/S0373463326101532 Published online by Cambridge University Press

$$\lambda_T = \lambda_D + D\lambda_T \tag{29}$$

$$\tan C_T = \frac{\sin\varphi_2 \cos\varphi_T - \cos\varphi_2 \sin\varphi_T \cos|\lambda_2 - \lambda_T|}{\cos\varphi_T \sin|\lambda_2 - \lambda_T|} \tag{30}$$

where $D\lambda_T$ is the difference in longitude from point D to point T; φ_T denotes the latitude of point T; λ_T is the longitude of point T; C_T represents the great-circle course at point T. As well as C_T represents the desired heading in the improved LOS algorithm.

Then, derived from the current ship placement, calculate the target point location and the great-circle course C_T, which is the desired course. There will be a difference between C_T and the ship's starting heading ψ, which is the course that needs to be adjusted. By progressively minimising the discrepancy between the intended course and the actual course of the ship, the vessel will follow the great-circle route.

3.3. Design of control system

The closed-loop gain shaping scheme, as a simplified engineering implementation of robust control, is characterised by its basic solution procedure and ease of engineering application. The controller designed with this method has strong robustness. In this paper, a third-order closed-loop gain-shaping method is used to layout the controller K. Let the bandwidth frequency of the closed-loop system be $1/T_1$, then the complementary sensitivity function T of the ship's course-conserving control structure, which is also the closed-loop transmit capacity of the mechanism, is

$$T = \frac{1}{(T_1 s + 1)^3} = \frac{G_{\psi\delta}(s)K}{1 + G_{\psi\delta}(s)K} \tag{31}$$

Then, the ultimate robust controller can be expressed as

$$K = \frac{T_0 \mathrm{s}+1}{K_0 T_1 (T_1{}^2 \mathrm{s}^2 + 3T_1 \mathrm{s} + 3)} = \left(\frac{T_0 \mathrm{s}}{K_0 T_1} + \frac{1}{K_0 T_1}\right)\left(\frac{1}{T_1{}^2 \mathrm{s}^2 + 3T_1 \mathrm{s} + 3}\right) \tag{32}$$

From Equation (32), it is evident that the structure of the controller resembles a typical proportional-derivative (PD) controller combined in series with an oscillatory component. This form is concise and very easy to implement, solving the problems of complex parameter tuning and unclear physical meaning associated with conventional PD controllers.

In practical operations, ships have large inertia, which requires a longer adjustment time for control. Under a PD controller, a constant ρ is introduced. This allows the system to significantly reduce the adjustment time without compromising stability. Analogous to this method, a positive constant can be added to the proportional part of the PD term in Equation (32). In this paper, based on simulation tests, the constant $\rho = 2$ is chosen to get the optimal performance, resulting in the final form of the controller as (Li and Zhang, 2023)

$$K = \left(\frac{T_0 \mathrm{s}}{K_0 T_1} + \frac{1}{K_0 T_1} + \rho\right)\left(\frac{1}{T_1{}^2 \mathrm{s}^2 + 3T_1 \mathrm{s} + 3}\right) \tag{33}$$

3.4. Coordinate transformation

The Mercator map projection is a widely adopted plane projection method for maritime chart creation. It enables the mapping of the Earth's curved surface onto a flat plane, thereby facilitating the use of nautical charts. A key feature of this projection is its preservation of course linearity; however, it substantially exaggerates areas near the poles, leading to significant distortions in high-latitude regions.

https://doi.org/10.1017/S0373463326101532 Published online by Cambridge University Press

A planar map (usually referring to a map in a Cartesian coordinate system) is typically represented based on a simple Cartesian coordinate system (such as x and y coordinates).

(1) Mercator Projection Coordinates Planar Coordinates Conversion. If the latitude and longitude of a point (φ, λ) are known, the following formula can be used to convert it to planar coordinates:

$$x = R\lambda \tag{34}$$

$$y = R\ln\left[\tan\left(\frac{\pi}{4} + \frac{\varphi}{2}\right)\right] \tag{35}$$

Here, R is the Earth's radius, typically taken as approximately 6371 km (if different units such as metres and miles are used, R also needs to be adjusted accordingly); x and y correspond to the Cartesian coordinates on the plane; λ, φ are the Mercator projection coordinates for longitude and latitude, respectively.

The longitude and latitude in the above formula need to be in radians. If the longitude and latitude data are in degrees, they first need to be converted to radians:

$$\lambda_{\text{radian}} = \lambda_{\text{angle}}\frac{\pi}{180} \tag{36}$$

$$\varphi_{\text{radian}} = \varphi_{\text{angle}}\frac{\pi}{180} \tag{37}$$

(2) Planar Coordinates to Mercator Projection Coordinates. If you already have the planar coordinates (x, y) and want to convert them back to the Mercator projection's latitude and longitude, you can use the inverse formula for conversion:

$$\lambda = \frac{x}{R} \tag{38}$$

$$\varphi = 2\arctan(e^{\frac{y}{R}}) - \frac{\pi}{2} \tag{39}$$

By converting the ship's position from planar coordinates to coordinates on a Mercator projection nautical chart, the guidance strategy can better meet the actual navigation requirements, as a result, the practicality and applicability of the control structure are improved.

4. Simulation verification

The simulation of the maritime path of the YUKUN from the Bahamas Islands (approximate position: latitude 24°48.0′N, longitude 75°48.0′W) to the Strait of Gibraltar (approximate position: latitude 36°00.0′N, longitude 5°12.6′W) was conducted. The main design parameters of the YUKUN are shown in Table 1. The initial ship's heading was set at 070° and wind conditions of Beaufort scale 6 were established. To reduce simulation time and accelerate the programme response speed, the radius of the Earth was reduced by a factor of 1000. In the simulations of this study, after multiple rounds of simulation validation, S_T is set to 200. The simulation tested the performance of three navigation methods, including the great-circle route guidance method proposed in this study, the LOS constant bearing guidance method and the LOS-based approximate great-circle segment guidance method. The simulation outcomes are presented in Figures 5 to 8.

The findings in Figure 5 indicate that all three navigation methods designed in this chapter – the great-circle route guidance method, the constant course guidance method based on LOS and the

https://doi.org/10.1017/S0373463326101532 Published online by Cambridge University Press

Table 1. *Main design particulars of 'Yukun' ship*

Name	Symbol	Unit	Yukun
Length between perpendiculars	L	m	105
Breadth	B	m	18
Design draught	d	m	5.4
Deadweight	DWT	t	5735.5
Centre of gravity	X_c	m	−0.51
Block coefficient	C_b	/	0.5595
Rudder area	$A\delta$	m^2	11.46
Design speed	V_0	kn	16.7

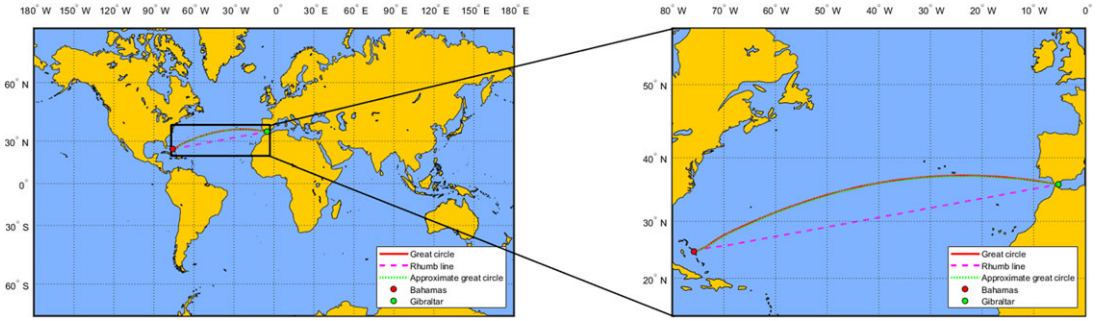


Figure 5. *Track comparison.*

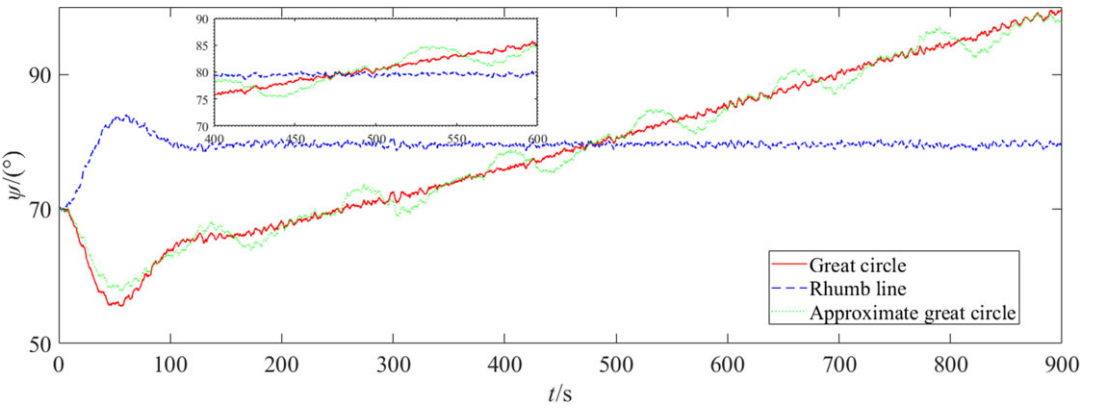


Figure 6. *Heading comparison.*

approximate great-circle segmented guidance method based on LOS – can all navigate stably along the planned route under the influence of Beaufort Scale 6 wind conditions.

From Figure 6, it can be observed that with the initial ship heading set to 070°, the heading adjustment behaviours of the three methods are as follows: the great-circle navigation method adopts an initial heading of 061.1°, whereas the constant course navigation method uses an initial heading of 079.5°. During the simulation, the initial heading of the ship is gradually adjusted. The great-circle navigation method began to stably track the reference heading after about approximately 100 s, after which the ship's heading increased uniformly with changes in position. The constant course navigation method stabilised in tracking the reference heading for approximately 100 s and then maintained a stable heading. In comparison, the approximate great-circle segmented navigation method requires heading

https://doi.org/10.1017/S0373463326101532 Published online by Cambridge University Press

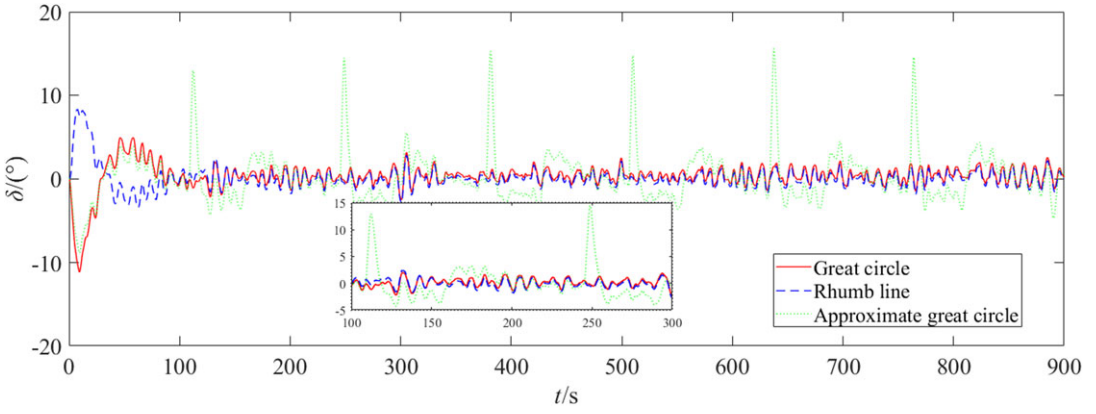


Figure 7. *Rudder angle comparison.*

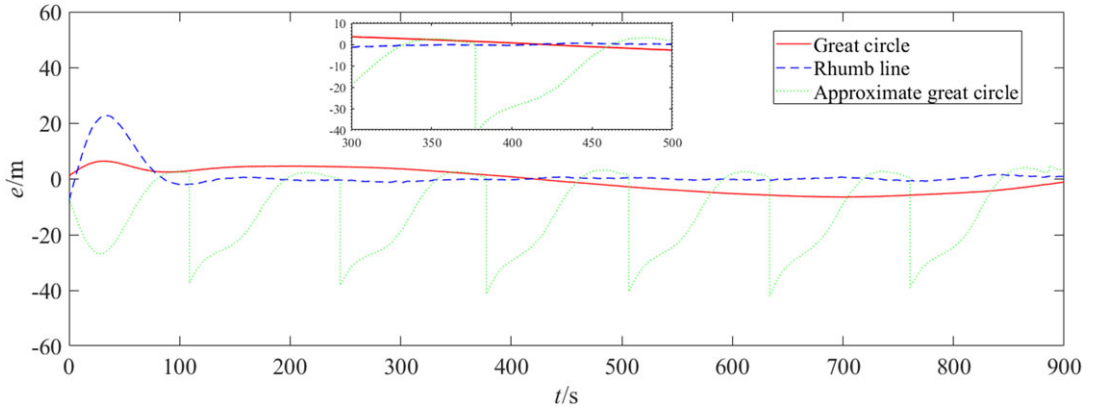


Figure 8. *Tracking error comparison.*

adjustments at each segment, resulting in continuous heading changes throughout the simulation. It is important to note that due to the reduction of the Earth's radius by a factor of 1,000 in the simulation, the heading adjustments for the segmented navigation method occur more frequently. In actual navigation, this frequency of adjustment would be significantly reduced.

As is shown in Figure 7, both the great-circle navigation approach and the constant course navigation method are primarily in the controller adjustment phase within the first 100 s, leading to more pronounced rudder angle variations. After about 100 s, the controller begins to stably track the reference signal and the rudder angle stabilises, with only minor adjustments made in response to high-frequency disturbances from waves. In contrast, the approximate great-circle segmented navigation method requires heading changes at each segment, leading to frequent and larger rudder angle adjustments throughout the entire simulation process.

Figure 8 further illustrates the changes in tracking deviation. In the early stages of the simulation, due to an initial heading difference of approximately 10° between the ship's initial heading and the reference heading, the ship needs to continuously adjust its heading to track the reference signal, resulting in a relatively large tracking deviation. However, after approximately 100 s of adjustment, the controller can stably follow the reference heading and the tracking error is substantially reduced. Throughout the entire navigation process, the maximum tracking error for the constant course guidance method based on LOS is approximately 25 m, while the maximum tracking error for the approximate great-circle segmented guidance method based on LOS is approximately 40 m. In contrast, the great-circle route guidance and

https://doi.org/10.1017/S0373463326101532 Published online by Cambridge University Press

Table 2. *Quantitative analysis after the simulation stabilizes*

Navigation method	Course change rate within 200 s	Maximum value of rudder angle variation (°)	Maximum value of route deviation (m)
Great circle	0.04	4.6	4.1
Rhumb line	0	5.5	1.1
Approximate great circle	0.08/−0.06	18.39	41.3

control strategy designed in this section achieves a maximum tracking error of only 6 m over the entire journey, demonstrating a significant advantage.

From Table 2, the value for the great circle remains constant because the course undergoes continuous linear variation. In contrast, the value for the rhumb line is 0 since there is no course change. For the approximate great circle, multiple values are observed due to the presence of course fluctuations. The great circle exhibits the smallest rudder angle variation, indicating the highest level of stability. Finally, although both the great circle and rhumb line exhibit deviations from the route, the variation amplitude of the great circle is smaller than that of the rhumb line in the initial phase. Meanwhile, the approximate great circle shows the largest variation amplitude among the three.

In summary, all three navigation methods are capable of effectively tracking great-circle routes under the same simulation environment. However, there are significant differences among them in terms of the frequency and magnitude of course adjustments, as well as the control of tracking errors. The great-circle navigation method and the loxodrome navigation method demonstrate relatively stable course-keeping control with fewer occurrences of abrupt rudder angle adjustments. In contrast, the segmented great-circle approximation method, which requires frequent course changes, results in larger rudder angle variations, thereby increasing the control complexity and the difficulty of operation. The control algorithm designed in this section has shown a distinct advantage in tracking accuracy, especially in terms of tracking error performance. Compared with the other two methods, the control method proposed in this section can navigate along the great-circle route with the smallest error and with a lower frequency of course adjustments in practical applications. This avoids frequent large-magnitude rudder angle adjustments, thereby enhancing the stability and reliability of navigation. These superior performance characteristics endow the control algorithm designed in this section with strong application potential in the field of navigation control, particularly for navigation tasks that require high-precision track keeping.

5. Conclusions

The guidance and control strategy for great-circle routes based on Mercator projection charts proposed in this paper successfully addresses the challenges of long voyages, the effects of Earth's curvature and the limitations of traditional navigation methods faced by ships during ocean navigation. By designing the guidance strategy for great-circle routes through the analysis of spherical triangles and combining it with a closed-loop gain-scheduling algorithm to achieve precise ship track-keeping control, this strategy overcomes the issue of traditional methods' inability to make real-time course adjustments during navigation, ensuring stable ship travel along the great-circle arc. Moreover, by transforming the ship's position from a planar map to a Mercator projection chart, the guidance strategy better meets the practical needs of maritime engineering, enhancing the applicability and practicality of the control system. This method not only improves the stability of ship travel along great-circle routes, but also effectively reduces navigation time and fuel consumption, thereby enhancing navigation efficiency and economy.

https://doi.org/10.1017/S0373463326101532 Published online by Cambridge University Press

6. Discussions

In the current simulation, only the wind force model has been incorporated to simulate the wind-induced effects on the ship. However, in actual marine environments, the impact of ocean waves is equally crucial for the ship. Future research can integrate a comprehensive wind-wave disturbance model to fully simulate the real operating conditions of ships at sea, thereby making the conclusions more consistent with practical scenarios. Furthermore, When the radius is reduced by 1,000 times, the Earth model becomes smaller and the curvature of the spherical surface increases significantly. This means that the originally long-distance route will appear more curved on the scaled-down model, with a more pronounced visual deviation from a straight line. Meanwhile, when the radius is reduced by 1,000 times, all distances calculated via spherical trigonometry will also be reduced by 1,000 times. Consequently, the relative impact of small errors in angle calculations will be amplified, which may lead to a decline in navigation accuracy. In future research, the real radius of the Earth can be adopted for calculations, which is more consistent with practical application scenarios.

However, since the actual Earth's surface is not a perfect sphere, the guidance algorithm based on a spherical model suggested in this study may face certain limitations in terms of accuracy during actual navigation. Future research can further optimise the guidance strategy by incorporating the Earth's ellipsoidal shape model and real-time data on environmental changes during navigation to improve the system's high-precision navigation capabilities. Meanwhile, the great circle route navigation method proposed in this paper is only applicable to scenarios within the same longitude zone (both the departure point and the destination are in the eastern longitude region or the western longitude region). Future research can extend to navigation scenarios crossing the 180° meridian and other broader application fields to achieve more comprehensive coverage of great-circle routes. Finally, due to the lack of an actual ship to verify the reliability of the proposed method, this paper only validates its feasibility through simulations. In future research, real-ship sea trials can be conducted to further confirm the feasibility of this method.

Acknowledgments. The authors would like to thank anonymous reviewers for their valuable comments to improve the quality of this article.

Funding statement. This work is partially supported by the National Natural Science Foundation of China [Grant No. 51679024], the Joint Program of Science and Technology Plan of Liaoning Province (Key Research and Development Program Project) [Grant No. 2025JH2/101800233], the Dalian Innovation Team Support Plan in the Key Research Field [Grant No. 2020RT08], the Basic Scientific Research Project of Liaoning Education Department [Grant No. LJ212410151025], and the 2023 DMU navigation college first-class interdisciplinary research project [Grant No. 2023JXA06].

References

Chen, C. L., Hsu, T. P. and Chang, J. R. (2004). A Novel Approach to Great Circle Sailings: The Great Circle Equation. *The Journal of Navigation*, **57**(2), 311–320. https://doi.org/10.1017/S0373463304002644

Chen, Y. L., Zhou, H., Zhao, Y. G. and Huo, J. Y. (2014). Fuzzy Robust Path Tracking Strategy of an Active Pelagic Trawl System with Coordinated Ship and Winch Regulation. *Journal of Central South University*, **21**(1), 167–179. https://doi.org/10.1007/s11771-014-1928-1

Dai, S., Wu, Z., Wang, J., Tan, M. and Yu, J. (2023). Barrier-Based Adaptive Line-of-Sight 3-D Path-Following System for a Multijoint Robotic Fish With Sideslip Compensation. *IEEE Transactions on Cybernetics*, **53**(7), 4204–4217. https://doi.org/10.1109/TCYB.2022.3155761

Do, K. D. (2016). Global Robust Adaptive Path-Tracking Control of Underactuated Ships Under Stochastic Disturbances. *Ocean Engineering*, **111**, 267–278. https://doi.org/10.1016/j.oceaneng.2015.10.038

Earle, M. A. (2005). Vector Solutions for Great Circle Navigation. *The Journal of Navigation*, **58**(3), 451–457. https://doi.org/10.1017/S0373463305003358

Fan, Y., Liu, B., Wang, G. and Mu, D. (2021). Adaptive Fast Non-Singular Terminal Sliding Mode Path Following Control for an Underactuated Unmanned Surface Vehicle with Uncertainties and Unknown Disturbances. *Sensors (Basel, Switzerland)*, **21**(22), 7454. https://doi.org/10.3390/s21227454

Fossen, T. I. (2022). Line-of-Sight Path-Following Control Utilizing an Extended Kalman Filter for Estimation of Speed and Course Over Ground From GNSS Positions. *Journal of Marine Science and Technology*, **27**(1), 806–813. https://doi.org/10.1007/s00773-022-00872-y

https://doi.org/10.1017/S0373463326101532 Published online by Cambridge University Press

Fu, M. and Wang, Q. (2023). Safety-Guaranteed, Robust, Nonlinear, Path-Following Control of the Underactuated Hovercraft Based on FTESO. *Journal of Marine Science and Engineering*, **11**(6), 1235. https://doi.org/10.3390/jmse11061235

Hondorp, D. W., Bennion, D. H., Roseman, E. F., Holbrook, C. M., Boase, J. C., Chiotti, J. A., Thomas, M. V., Wills, T. C., Drouin, R. G., Kessel, S. T. and Krueger, C. C. (2017). Use of Navigation Channels by Lake Sturgeon: Does Channelization Increase Vulnerability of Fish to Ship Strikes? *PloS One*, **12**(7), e0179791. https://doi.org/10.1371/journal.pone.0179791

Kim, D., Song, S., Turnock, S. and Tezdogan, T. (2023). Nonlinear URANS Model for Path-Following Control Problem Towards Autonomous Marine Navigation under Wave Conditions. *Ocean Engineering*, **270**, 113681. https://doi.org/10.1016/j.oceaneng.2023.113681

Kjerstad, Ø. K. and Coates, E. M. (2024). Enhancing Line-of-Sight Guidance to Improve Path Following for Marine Surface Vessels. *IFAC-PapersOnLine*, **58**(20), 1–8. https://doi.org/10.1016/j.ifacol.2024.10.024

Lan, J., Zheng, M., Chu, X. and Ding, S. (2023). Parameter Prediction of the Non-Linear Nomoto Model for Different Ship Loading Conditions Using Support Vector Regression. *Journal of Marine Science and Engineering*, **11**(5), 903. https://doi.org/10.3390/jmse11050903

Lee, S. D., Song, Y. S., Kim, D. H. and Kang, M. R. (2022). Path Following Control of an Underactuated Catamaran for Recovery Maneuvers. *Sensors (Basel, Switzerland)*, **22**(6), 2233. https://doi.org/10.3390/s22062233

Li, G. and Zhang, X., (2023). Green Energy-Saving Robust Control for Ship Course-Keeping System based on Nonlinear Switching Feedback. *Ocean Engineering*, **268**, 113462. https://doi.org/10.1016/j.oceaneng.2022.113462

Li, H., Liu, Z., Huang, J., An, X. and Chen, Y. (2025). An Improved ESO-based Line-of-Sight Guidance Law for Path Following of Underactuated Autonomous Underwater Helicopter with Nonlinear Tracking Differentiator and Anti-Saturation Controller. *Ocean Engineering*, **322**, 120456. https://doi.org/10.1016/j.oceaneng.2025.120456

Li, J., Zhang, G., Zhang, W., Shan, Q. and Zhang, W. (2024). Cooperative Path Following Control of USV-UAVs Considering Low Design Complexity and Command Transmission Requirements. *IEEE Transactions on Intelligent Vehicles*, **9**(1), 715–724. https://doi.org/10.1109/TIV.2023.3317336

Liu, C., Li, T., Wu, W., Zheng, H., Li, J. and Chu, X. (2024a). Event-Triggered Predictive Path Following Control of Autonomous Ships with an MMG Model. *Ocean Engineering*, **314**, 119582. https://doi.org/10.1016/j.oceaneng.2024.119582

Liu, J., Huang, L., Yu, D., Xu, L. and He, Y. (2024b). The Control Method for Ship Tracking When Navigating Through Narrow and Curved Sections. *Applied Ocean Research*, **145**, 103943. https://doi.org/10.1016/j.apor.2024.103943

Liu, X., Ren, S., Zhang, L., Shen, W. and Tu, Y. (2023). Research on Dynamic Path Planning and Tracking Control for Ship Collision Avoidance. *Journal of Physics: Conference Series*, **2607**(1), 012012. https://doi.org/10.1088/1742-6596/2607/1/012012

Liu, X. and Zhang, W. (2024). Prescribed Performance Actuator-Tolerance Control for Path Following of Unmanned Surface Vessels via the Triggered Adaptive Line-of-Sight Guidance. *Computers and Electrical Engineering*, **120**, 109617. https://doi.org/10.1016/j.compeleceng.2024.109617

Lu, S., Wang, B., Dong, Z., Hu, Z., Ding, Y. and Liu, W. (2024). Parameter Identification of an Unmanned Surface Vessel Nomoto Model Based on an Improved Extended Kalman Filter. *Applied Sciences*, **15**(1), 161. https://doi.org/10.3390/app15010161

Martinsen, A. B., Lekkas, A. M., Gros, S., Glomsrud, J. A. and Pedersen, T. A. (2020). Reinforcement Learning-Based Tracking Control of USVs in Varying Operational Conditions. *Frontiers in robotics and AI*, **7**, 32. https://doi.org/10.3389/frobt.2020.00032

Meng, Y., Wu, Z., Chen, D., Zhang, P., Tan, M. and Yu, J. (2024). Development and 3-D Path-Following Control of an Agile Robotic Manta With Flexible Pectoral Fins. *IEEE Transactions on Cybernetics*, **54**(6), 3727–3738. https://doi.org/10.1109/TCYB.2023.3252589

Mo, Y., Su, W., Hong, Z., Li, Y. and Zhong, Y. (2024). Finite-Time Line-of-Sight Guidance-Based Path-Following Control for a Wire-Driven Robot Fish. *Biomimetics*, **9**(9), 556. https://doi.org/10.3390/biomimetics9090556

Stuart, R. G. (2017). Great Circles and Rhumb Lines on the Complex Plane. *The Journal of Navigation*, **70**(3), 618–627. https://doi.org/10.1017/S0373463316000886.

Tanakitkorn, K., Phoemsapthawee, S., Thaweewat, N., et al. (2024). Unified Line-of-Sight: A Guidance Algorithm with Integral Wind-Up Mitigation and Turning assist for USVs. *Ocean Engineering*, **314**: 119615. https://doi.org/10.1016/j.oceaneng.2024.119615

Yin, J. and Wang, N., (2021). Predictive Trajectory Tracking Control of Autonomous Underwater Vehicles Based on Variable Fuzzy Predictor. *International Journal of Fuzzy Systems*, **23**(6), 1809–1822. https://doi.org/10.1007/s40815-020-00898-7

Yu, C., Liu, C., Xiang, X., Zeng, Z., Wei, Z. and Lian, L. (2020). Line-of-Sight Guided Time Delay Control for Three-Dimensional Coupled Path Following of Underactuated Underwater Vehicles with Roll Dynamics. *Ocean Engineering*, **207**, 107410. https://doi.org/10.1016/j.oceaneng.2020.107410

Zhang, H., Zhang, X., Xu, H. and Guedes Soares, C. (2024). Heterogeneous Cooperative Trajectory Tracking Control between Surface and Underwater Unmanned Vehicles. *Ocean Engineering*, **301**, 117137. https://doi.org/10.1016/j.oceaneng.2024.117137

Zhang, Q., Zhang, M., Hu, Y. and Zhu, G. (2020). Error-Driven-based Adaptive Nonlinear Feedback Control of Course-Keeping for Ships. *Journal of Marine Science and Technology*. (2020)[2025-12-02]. https://doi.org/10.1007/s00773-020-00741-6

https://doi.org/10.1017/S0373463326101532 Published online by Cambridge University Press

Zheng, H., Hu, Q., Yang, C., Chen, J. and Mei, Q. (2021). Transmission Path Tracking of Maritime COVID-19 Pandemic via Ship Sailing Pattern Mining. *Sustainability*, **13**(3), 1089. https://doi.org/10.3390/su13031089.

Zhu, G., Xu, Z., Gao, Y., Yu, Y. and Li, L. (2025). Periodic Event-Triggered Adaptive Neural Output Feedback Tracking Control of Unmanned Surface Vehicles Under Replay Attacks. *Engineering Applications of Artificial Intelligence*, **146**, 110237. https://doi.org/10.1016/j.engappai.2025.110237

Cite this article: Li, G., Li, G., Zhang, X., Wang, S., and Xie, Z. (2026). Line-of-sight based great-circle route track-keeping control. *The Journal of Navigation* **79**: 1-2, 40–55. https://doi.org/10.1017/S0373463326101532

https://doi.org/10.1017/S0373463326101532 Published online by Cambridge University Press